4-13-2016

Development of Reduced Chemistry for Efficient Combustion Simulations

Yufeng Liu
yufengliu812@gmail.com

Development of Reduced Chemistry for Efficient Combustion Simulations

Yufeng Liu

B.E., University of Science and Technology of China, 2012

A Thesis

Submitted in Partial Fulfillment of the

Requirements of the Degree of

Master of Science

At the

University of Connecticut

2016

Approval Page

Master of Science Thesis

Development of Reduced Chemistry for Efficient Combustion Simulations

Presented by

Yufeng Liu, B.E.

Major Advisor _____
Tianfeng Lu

Associate Advisor _____
Baki Cetegen

Associate Advisor _____
Xinyu Zhao

University of Connecticut

2016

Acknowledgements

I would like to express my appreciation to my advisor, Prof. Tianfeng Lu, for giving me opportunity to participate in the combustion research at the University of Connecticut (UCONN). His advice and support made this work possible.

I am also sincerely grateful to my co-advisors Prof. Baki Cetegen and Prof. Xinyu Zhao for reviewing my thesis and providing insightful comments. I also want to thank Prof. Zhuyin Ren in Tsinghua University for his advisory during my first year at UConn.

My gratitude also goes to my colleagues and friends at UCONN: Chao Xu, Angran Li, Cong Li, Dr. Pengfei Li, Bifen Wu, Dr. Zhaoyu Luo, Dr. Ruiqin Shan, Hongtao Yang, Dr. Xianming Wang, Yang Gao, Yunchao Wu, Mike Kuron, Dr. Tong Yao, Brian Magda and Ji-Woong Park. Their help made my study at UCONN a great pleasure. The same appreciation is for Dr. Peng Zhao in Oakland University for his encouragement and help.

Very special thanks to my parents, Yong Liu and Yun Shao for their endless and unconditional love and support.

Table of Contents

Abstract

Detailed chemical kinetics is important for high-fidelity reacting flow simulations. The major challenge of incorporation of detailed chemistry in large-scale simulations is primarily attributed to the high computational cost, induced by the large number of species and reactions, as well as the severe chemical stiffness. Methodologies are therefore needed to facilitate the use of detailed chemistry in large-scale combustion simulations. In the present study, a linearized error propagation (LEP) model is developed to eliminate unimportant species and reactions from detailed chemistry. In the LEP model, the reduction errors are analytically approximated and formulated for perfectly stirred reactors (PSR). The performances of LEP in development of local and global reduced models are compared with previous approaches including directed relation graph (DRG) and DRG with error propagation (DRGEP). It was shown that LEP can effectively control the reduction errors in selected target species and global flame properties, such as ignition delay time. The skeletal models obtained by LEP are validated in PSR, auto-ignition and 1-D premixed flames.

Chemistry calculations can be further accelerated through dynamic adaptive chemistry (DAC) and *in-situ* adaptive tabulation (ISAT). DAC can expedite the time integration of chemical kinetics by using local skeletal models that can be substantially smaller than global skeletal models. ISAT can reduce the number of time integration by tabulating and re-using the previous solutions. Their relative performances are investigated for homogeneous charge compression ignition (HCCI) combustion and partially-stirred reactors (PaSR). It was shown that, compared to ISAT, the performance of DAC is mostly independent of the nature of combustion simulations, e.g., steady or unsteady, premixed or non-premixed combustion, and its efficiency increases with the size of chemical kinetic models. DAC is particularly suitable for

transient combustion simulations with large chemistry models, while ISAT can be more efficient for simulations where chemistry calculations can be frequently retrieved from the ISAT table. Moreover, a combined approach of ISAT and DAC, namely ISAT-DAC, is developed and demonstrated to accelerate the chemistry calculations. The incurred errors in temperature and species concentrations by ISAT-DAC are well controlled and the performance of ISAT is shown significantly enhanced by DAC.

Chapter 1 Introduction

1.1 Motivation

Combustion is an important energy conversion process that significantly impacts almost every aspects of the society. Fossil fuel consumption contributes to more than 80% of the global energy consumption and will remain as the primary energy source in the foreseeable future, while it is also the major source of pollutant emissions, such as nitrogen oxides, unburned hydrocarbons and particle matters. It is challenging to design efficient combustion devices that also feature low emissions. Computational fluid dynamics (CFD) plays an important role in understanding the flame behaviors and the subsequent design and optimization of engine combustors. Compared to experiment approaches, numerical simulations can be performed with reduced cost and can also provide detailed flow and chemical information that is difficult to access in experimental diagnostics.

Accurate description of chemistry is critical for predicting oxidation processes and pollutant emissions involving complex flow-chemistry couplings, e.g. in flame propagation, ignition and extinction problems. While comprehensive detailed chemistry models have been developed for a variety of fuels, it is challenging to incorporate the detailed chemistry models in large-scale combustion simulations. A detailed chemistry of hydrocarbon fuels can consist of thousands of species and reactions, which induce significant computational costs. In addition, the chemical timescales are vastly different ranging from sub-nanoseconds to seconds and the resulting chemical stiffness renders the low-cost explicit integration solvers inapplicable for many simulations [1]. Therefore efficient approaches are needed to accommodate detailed chemistry in reactive flow simulations.

1.2 Background

In the past a few decades, significant progress has been made in methodologies to facilitate the implementation of detailed chemistry in reactive flow simulations. The frequently used approaches include: skeletal chemistry reduction [2-12], timescale analysis techniques [13-21], dynamic adaptive chemistry (DAC) [22-25] and storage-retrieval methodologies [26-30] such as *in-situ* adaptive tabulation (ISAT) [28,29].

1.2.1 DRG-based skeletal model reduction

Skeletal reduction for detailed chemistry model can be achieved by eliminating unimportant species and reactions from detailed chemistry. The methods for skeletal reduction have been extensively studied, and the DRG-based methods have been shown to be particularly efficient and robust for reduction of large chemistry models of hydrocarbon fuels. In DRG [2,12], species couplings are mapped to a digraph and the species strongly coupled to selected species can be identified using a linear-time graph search [31]. DRG defines a pair-wise error, r_{AB}, to quantify the coupling between species, which is the relative error directly induced to species A by removing another species B:

$$r_{AB} \equiv \frac{\max_i |\nu_{A,i}\omega_i\delta_{Bi}|}{\max_i |\nu_{A,i}\omega_i|}, \quad \delta_{Bi} = \begin{cases} 1, & \text{if the ith reaction involves B} \\ 0, & \text{otherwise} \end{cases} \tag{1-1}$$

where subscript i donates the ith reaction, ω_i is the net reaction rate and $\nu_{A,i}$ is the stoichiometric coefficient of species A in the ith reaction. There is an edge from species A to B if and only if r_{AB} is larger than a user-specified threshold $\varepsilon_{\mathrm{DRG}}$, expressed in graph notation as

$$A \to B \text{ iff } r_{AB} > \varepsilon_{\mathrm{DRG}} \tag{1-2}$$

Another widely used method for skeletal reduction is DRGEP [7], in which a different coupling coefficient is defined:

$$r_{AB} \equiv \frac{\left|\sum_{i=1,K}(\nu_{A,i}\omega_i\delta_{B,i})\right|}{\max(P_A, C_A)} \tag{1-3a}$$

$$P_A = \sum_{i=1,I} \max(\nu_{A,i}\omega_i, 0) \tag{1-3b}$$

$$C_A = \sum_{i=1,I} \max(-\nu_{A,i}\omega_i, 0) \tag{1-3c}$$

where P_A and C_A are the production and consumption fluxes, respectively, and r_{AB} is bounded between 0 and 1. Starting form vertex S_1 to S_n along a path *p*, the coefficient in DRGEP is defined as:

$$r_{AB,p}^{DRGEP} = \prod_{i=1,n-1} r_{S_iS_{i+1}} \tag{1-4}$$

where *n* indicates the n^{th} vertex on the path, and

$$r_{AB}^{DRGEP} = \max_p(r_{AB,p}^{DRGEP}) \tag{1-5}$$

It is seen that the major difference between DRGEP and DRG is that DRGEP assumes that error geometrically decays along the graph paths, while DRG assumes that errors do not decay along the graph paths. Such difference in error propagation significantly affects the error control performance in DRG and DRGEP. It was shown that DRGEP can effectively control the reduction errors only in the target parameters, while DRG can control the worst-case errors in all the retained species [32].

1.2.2 In-situ adaptive tabulation (ISAT)

ISAT tabulates solutions of time integration of the chemical source term and returns approximated solutions when queried, and the ISAT table is generated on-the-fly. The ISAT table is empty at the beginning of the simulation. The table entries, referred to as leaves, are added as needed based on query compositions generated by simulations. In each leaf, the

tabulated data includes its location in the composition space, $\boldsymbol{x}$, the function value, $\boldsymbol{f}$, the sensitivity mapping matrix, $\boldsymbol{A}$, defined as $A_{ij} = \partial f_i/\partial x_j$, and information related to linear approximation error control. The approximation error is the direct two-norm difference between the linear approximation value, $\boldsymbol{f}^l$, and function value, i.e. $|\boldsymbol{f} - \boldsymbol{f}^l|$. Such an error returned by ISAT is normalized and smaller than a user specified error tolerance, $\varepsilon_{\mathrm{ISAT}}$. The domain, in which the linear approximation error is smaller than the threshold, is defined as the region of accuracy (ROA) and is modeled by the ellipsoid of accuracy (EOA). ISAT table has a data structure of binary tree for efficient searching. A leaf in the table is connected with another by a node in the upper level. The two leaves at $\boldsymbol{x}_1$ and $\boldsymbol{x}_2$ connected by the same node are separated by a cutting plane between them. The plane is unique, crosses the middle point between $\boldsymbol{x}_1$ and $\boldsymbol{x}_2$ and is normal to the vector $\boldsymbol{x}_1 - \boldsymbol{x}_2$. Information about the cutting plane and direction of both leaves is stored in the node.

ISAT has been implemented for efficient chemistry calculations in large-scale reactive flow simulations. In practical applications using ISAT, $\boldsymbol{x}$ represents the local thermochemical states of a particle or cell at the beginning of a reaction step of Δt, and $\boldsymbol{f}$ is the composition at the end of the integration step at adiabatic and isobaric condition. The evaluation of $\boldsymbol{f}(\boldsymbol{x})$ typically involves numerical integration of the set of $\boldsymbol{n_f}$ stiff ODEs. Based on a query, $\boldsymbol{x}^q$, the basic operations performed in ISAT are listed:

1. Retrieval: If the query point falls within the ellipsoid of accuracy (EOA) of $\boldsymbol{x}$, ISAT returns the linear approximation to $\boldsymbol{f}(\boldsymbol{x}^q)$ based on that leaf. When the retrieval event is successful, the operation is called a “retrieve”.
2. Growth: If a retrieval attempt fails, $\boldsymbol{f}(\boldsymbol{x}^q)$ is directly assessed by numerical integration and returned. Growth is attempted on some selected leaves close to $\boldsymbol{x}^q$. The linear

approximation error to $\boldsymbol{f}(\boldsymbol{x}^q)$ is evaluated for each of these selected leaves, and the leaf's EOA is grown to cover $\boldsymbol{x}^q$ if the error is less than ε_{ISAT}. If one growth attempt is successful at least, this operation is defined as a "grow".

3. Addition: If all the growth attempts fail and the allowed memory limit of ISAT table has not been reached, a new leaf of $\boldsymbol{x}^q$ is added to the ISAT table. This operation is referred to an "add".
4. Discarded evaluation: If an addition attempt is not successful due to insufficient memory in the ISAT table, $\boldsymbol{f}(\boldsymbol{x}^q)$ obtained by the integration is returned without further action. This operation is called a "discard" and it does not affect the ISAT table.

One operation of growth, addition or discarded evaluation involves one ODE integration, whose CPU time, t_F, is typically larger than that of a "retrieve", t_R, by several order of magnitude. When the reaction solutions tabulated in the ISAT table are retrieved, the chemistry calculation is accelerated, and thus the performance of ISAT depends on the fraction of "retrieve", p_R, in a simulation. The memory of ISAT table, the number of performed queries and the nature of the simulation may affect the fractions of different operations. Denote p_F as the sum of the probabilities of "grow", "add" and "discard", the average CPU time for a query, t_Q is approximately calculated:

$$t_Q = t_R p_R + t_F p_F = t_R(1 - p_F) + t_F p_F, \tag{1-6}$$

and the speedup factor in chemistry calculation is

$$\gamma = \frac{t_F}{t_Q} = \frac{1}{p_F + (1 - p_F)t_R/t_F} \tag{1-7}$$

The ideal speedup factor for ISAT is $\gamma = t_F/t_R$, which occurs when p_R approaches one, i.e., nearly all the evaluation are returned by "retrieve". In contrast, the performance deteriorates when p_R approaches zero.

In the present study, a linearized error propagation (LEP) model for skeletal reduction and a dynamic adaptive chemistry (DAC) approach based on DRG are developed to allow for efficient use of detailed chemistry in large-scale combustion simulations. The DAC method is further integrated with ISAT to achieve high speedup factors.

1.3 Organization of the thesis

Chapter 2 introduces the LEP model for skeletal reduction. The results show that LEP is more effective in control the reduction error in selected target species compared with DRG and DRGEP. Chapter 3 focuses on the application of ISAT and DAC for efficient reactive flow simulations. The relative performances of ISAT and DAC are compared in test cases including homogeneous charge compression ignition (HCCI) and partially-stirred reactors (PaSR). An efficient combined method of ISAT-DAC is developed and tested in PaSR.

Chapter 2 A linearized error propagation model for chemistry model reduction

2.1 Introduction

Detailed chemistry models for practical hydrocarbon fuels can involve a large number of species and reactions. Chemistry model reduction is thus needed for efficient flame simulations involving detailed chemistry model. Chemistry model reduction can be achieved through timescale analysis and skeletal reduction etc., as reviewed in [31]. Timescale analysis is typically based on the observation that fast processes become exhausted after a transient period and the fast species can be related with the slow ones by algebraic equations. Timescale based reduction methods include, for example, quasi steady state approximation (QSSA) [19-21], computational singular perturbation (CSP) [15], rate-controlled constrained equilibrium (RCCE) [13,14] and intrinsic low-dimensional manifold (ILDM) [16]. Skeletal reduction eliminates unimportant species and reactions from detailed chemistry, and can be achieved through such methods as sensitivity analysis [10], principle component analysis (PCA) [11], and directed relation graph (DRG) [2-4] and other DRG based methods such as DRGEP [7] and PFA [8]. The DRG based methods can also be combined with sensitivity analysis, e.g. in DRG-aided sensitivity analysis (DRGASA) [33] and DRGEP and sensitivity analysis (DRGEPASA) [34].

Among all the skeletal reduction methods, DRG and DRGEP are two typical methods frequently used in static and on-the-fly reduction. DRG was found to feature a linear reduction time and effectively control the reduction error in all the retained species. DRGEP was shown to effectively control errors in the species adjacent to the target species in the graph and can be infective in controlling the reduction errors in the species many steps away from the starting

species because of the rather aggressive assumption that the reduction errors geometrically decay along the graph paths.

Since accurate estimation of error propagation can help to obtain smaller chemistry models while the same level of reduction errors in species of interest is retained, a linearized error propagation (LEP) model is proposed in the present study to analytically estimate the error propagation based on Jacobian analysis in steady-state perfectly stirred reactors (PSR). The obtained skeletal models are then tested in PSR, auto-ignition and laminar premixed flame propagation.

2.2 Methodology

2.2.1 Steady-state perfectly stirred reactors

Skeletal reduction typically requires sampling of chemical reaction states from representative 0-D and 1-D flames, such as auto-ignition, PSR, 1-D premixed and non-premixed flames. Previous studies demonstrated that in most cases the skeletal models derived from auto-ignition and PSR can be extended to more complex flames [31]. Auto-ignition is a representative ignition application and PSR is a typical application involving flame chemistry and extinction. As such the combined sample dataset can be rather comprehensive and the resulting reduced models can be frequently extended to predict more complex flame behaviors, such as flame speed and flame extinction.

A steady-state PSR is a 0-D reactor that features the *S*-cure behavior [35]. Figure 2-1 shows the PSR response curves for stoichiometric ethylene/air mixture with inlet temperature of 1000 K at different pressures using the 111-species USC-Mech II [36]. The upper turning points on the curves are the extinction points controlled by high temperature chemistry, and the low

turning points are ignition points controlled by ignition chemistry [37,38]. In the present study, reduction solely based on PSR solutions will be explored and the sampling from auto-ignition will be replaced by that near the ignition states of PSR. A new linearized error propagation (LEP) model is formulated particularly for PSR, while the validation of obtained skeletal chemistry models will be extended to other flames.

2.2.2 Skeletal reduction based on LEP on PSR

The governing equations for steady state PSR can be expressed as:

$$\boldsymbol{\omega}(\boldsymbol{y}) + \boldsymbol{s}(\boldsymbol{y}) = 0$$

$$\omega_i(\boldsymbol{y}) = \dot{m}_i/\rho,\ i = 1, 2, \dots, n_s, \quad \omega_{n_s+1}(\boldsymbol{y}) = -\sum_{i=1,n_s} \dot{m}_i h_i\ /(\rho c_p) \tag{2-1}$$

$$s_i(\boldsymbol{y}) = (Y_i^0 - Y_i)/\tau,\ i = 1, 2, \dots, n_s,\ s_{n_s+1}(\boldsymbol{y}) = \sum_{i=1,n_s} Y_i^0 (h_i^0 - h_i)\ /(\tau c_p)$$

where $\boldsymbol{y}$ is a vector of dependent variables, including species mass fractions, $\boldsymbol{Y}$, and temperature, T. The subscript i indicates the ith species, the superscript *0* indicates the inlet condition, n_s is the total number of species, ρ is density, $\dot{m}$ is the mass production rate, c_p is constant pressure heat capacity, h is the specific enthalpy, and τ is the residence time for a particle in PSR. The $(n_s + 1)th$ variable in $\mathbf{y}$ is temperature.

In the LEP model, a species is defined as a minor species if it is in low concentration compared to a threshold value, say mass fraction being smaller than 10^{-3}. After eliminating a minor species, say the L^{th} with the mass fraction donated as Y_L, the governing equations of PSR can be formulated as:

$$\frac{\boldsymbol{Y}' - \boldsymbol{Y}^0}{\tau} = \boldsymbol{\omega}'(\boldsymbol{Y}')$$
$$\boldsymbol{\omega}'(\boldsymbol{Y}') = \boldsymbol{\omega}(\boldsymbol{Y}', Y_L) - \boldsymbol{\omega}^L(\boldsymbol{Y}', Y_L) \tag{2-2}$$

where $\boldsymbol{Y}'$ is the steady state PSR solution without Y_L, $\boldsymbol{\omega}'$ indicates the chemical source term after eliminating species L and $\boldsymbol{\omega}^L$ indicates the chemical source term attributed to the reactions involving species L. The reduction errors in the remaining species induced by the removed species L are thus approximated using the following linearized model:

$$\delta\boldsymbol{Y} = \boldsymbol{Y} - \boldsymbol{Y}' \approx \left(\frac{\boldsymbol{I}}{\tau} - \boldsymbol{J}_{\boldsymbol{\omega}'}\right)^{-1} \boldsymbol{\omega}^L(\boldsymbol{Y}, Y_L), \qquad \boldsymbol{J}_{\boldsymbol{\omega}'} = \frac{\partial \boldsymbol{\omega}'}{\partial \boldsymbol{Y}} \tag{2-3}$$

The Jacobian matrix, $\boldsymbol{J}_{\boldsymbol{\omega}'}$, is analytically evaluated in the present study for maximal precision and high efficiency.

In the use of LEP for chemistry model reduction, only errors in some selected species of interest are controlled. The target species usually include the species in high mass fractions, the fuel, important radicals, and pollutant species of interest. The reduction errors in the target species are compared with a user-specified threshold value to determine whether a minor species can be eliminated.

2.3 Results and discussions

The LEP-based chemistry model reduction is first performed on PSR solutions of ethylene/air mixtures with inlet temperature of 1000 K at equivalence ratios of 0.5, 1.0 and 1.5 and pressures of 1, 5 and 30 atm using USC-Mech II. The target species include the local major species with mass fraction greater than 10^{-3}, the fuel and H radical. The sampled reaction states from PSR cover a wide range of flame conditions involving ignition, extinction and strongly burning states. A local skeletal model is derived for each sampled reaction state using error

thresholds similar to those used in DRG and DRGEP. Note that the updated formulation of DRG by Luo et al. [12] is adopt in the present study. The reduction errors are measured using PSR solutions at fixed temperatures with species mass fractions and residence time as dependent variables. The relative error in the mass fraction of the i^{th} species is defined as:

$$\varepsilon_i = \frac{|Y_i - Y_i'|}{|Y_i| + |Y_i'|} \tag{2-4}$$

Figure 2-2 shows the worst-case relative errors in the major species and H radical as function of the threshold values for local chemistry models obtained by LEP, DRG and DRGEP, respectively. The dashed lines show the 1:1 correlation between measured relative errors and the threshold values. It is seen that the measured errors from DRG are overall lower than the threshold, while the errors from LEP and DRGEP are close to the dashed lines. It indicates that the LEP and DRGEP can effectively control the reduction errors in the selected target species. In contrast, DRG typically over-controls the reduction errors in the target species since DRG controls the worst-case errors in all the remaining, rather than a selected set of, species as shown in [32]. It is further seen that the errors from LEP are overall smaller than those from DRGEP. While the differences in the incurred errors are insignificant in some major species as shown in Fig. 2-2a, significant difference in observed in H radical as shown in Fig. 2-2b, showing that the LEP model can better estimate the error propagation compared with the aggressive geometrically decaying model in DRGEP.

A global skeletal chemistry model valid for different reaction states can be further obtained by combining the local skeletal models derived from each reaction state. For demonstration, the LEP method is applied on PSR solutions of ethylene/air at pressures of 1, 5 and 30 atm, equivalence ratios of 0.5, 1.0 and 1.5, and initial temperatures of 300, 1000, 1200, 1400 and 1600 K. Ignition states are sampled from PSR solutions on the lower and middle

branches of the S-curves with T_{in} = 1000 – 1600 K, and reaction states for extinction flame chemistry are sampled from the middle and upper branches with T_{in} = 300 K. The global skeletal models obtained by LEP are compared with those by DRG and DRGEP, which are derived by sampling the corresponding auto-ignition solutions with the same parameter space.

Figure 2-3 shows the number of species in skeletal models as function of the threshold values for the three methods. With the same threshold, LEP can typically result in the smallest skeletal models, while the sizes of the models obtained by DRG are the largest. Figure 2-4 shows the worst-case errors in ignition delay time as function of the number of species in the skeletal models obtained by DRG, DRGEP and LEP, respectively, and it is seen that LEP achieves the lowest reduction curve. It is noted that in DRG, some strongly coupled species may share the same threshold value and they are eliminated as a group in the test cases.

LEP is further applied to obtain a compact global skeletal model for ethylene using the PSR solutions with the above parameter range. A 45-species skeletal model was first derived using LEP with a small threshold 0.1. LEP reduction is then applied iteratively to obtain a compact skeletal model. Specifically, LEP eliminates the species giving the largest reduction error at each iteration step, and the reduction terminates if the incurred relative error in ignition delay time or extinction residence time of PSR is greater than 20%. As such the error incurred by the skeletal model is controlled in the monitored global behaviors with 20% error threshold. Note that such an iterative approach is similar to the DRG aided sensitivity analysis (DRGASA) approach [33]. A 34-species skeletal model with 197 elementary reactions is eventually obtained using LEP. The validation of the global skeletal model is shown in Fig. 2-5. It is seen that good agreement is achieved. The worst-case relative error in auto-ignition delay time and PSR extinction residence time is around 17%.

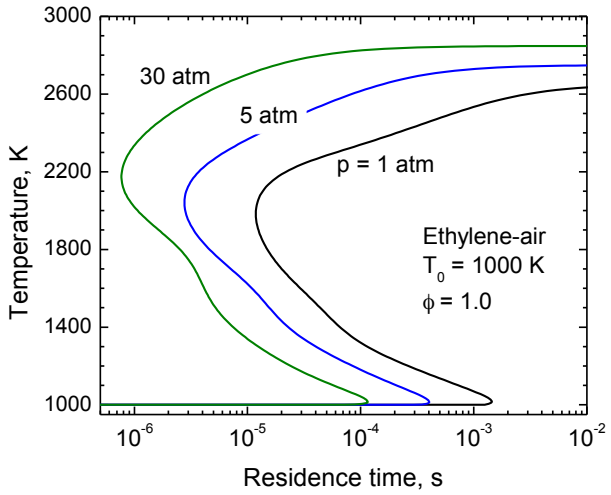

Figure 2-1. *S*-curve of PSR for stoichiometric ethylene-air mixtures at inlet temperature of 1000 K and different pressures, calculated using USC-Mech II [36].

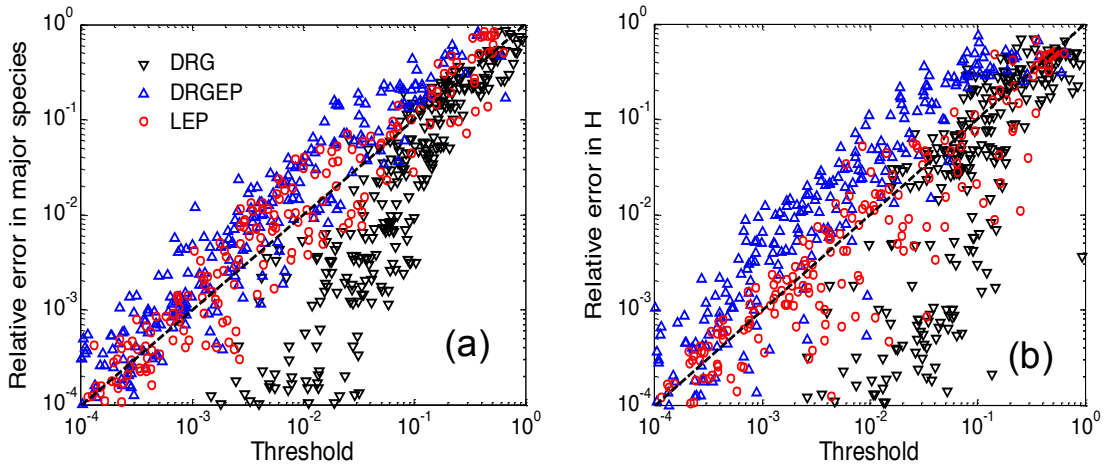

Figure 2-2. The worst-case relative errors in (a) major species and (b) H radical as function of the threshold value. Dashed lines are the 1:1 trend lines.

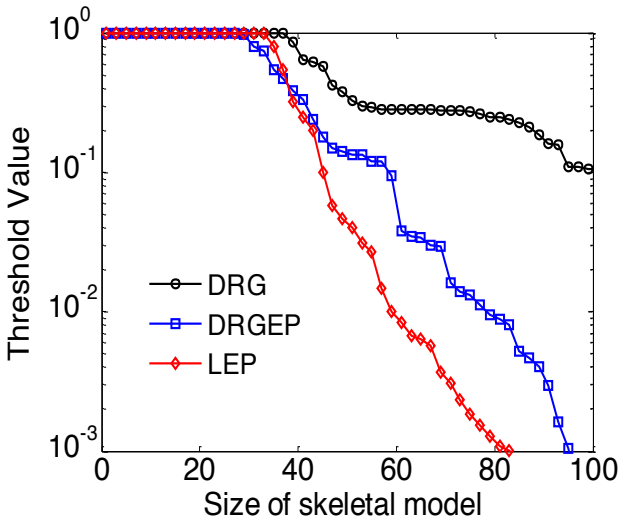

Figure 2-3. The number of species in the skeletal model as function of the threshold values for DRG, DRGEP and LEP, respectively.

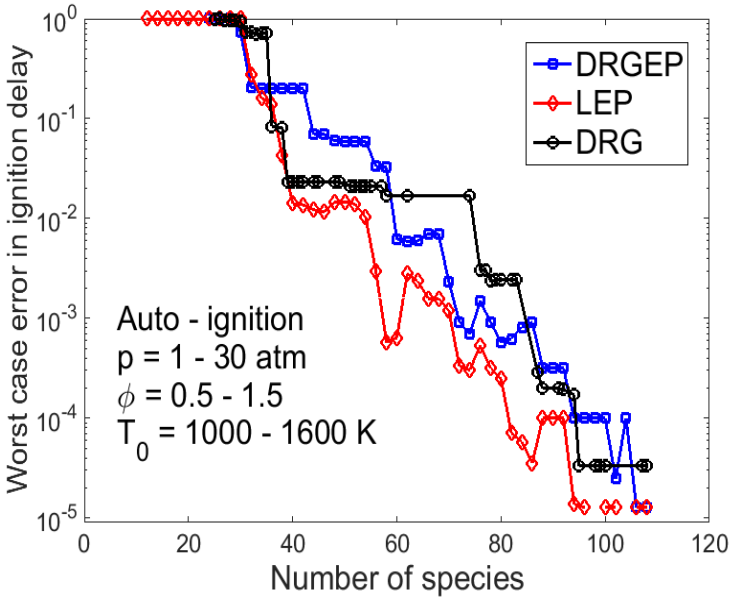

Figure 2-4. The worst-case relative errors in ignition delay time as function of the number of species in the skeletal models obtained using DRG, DRGEP and LEP, respectively.

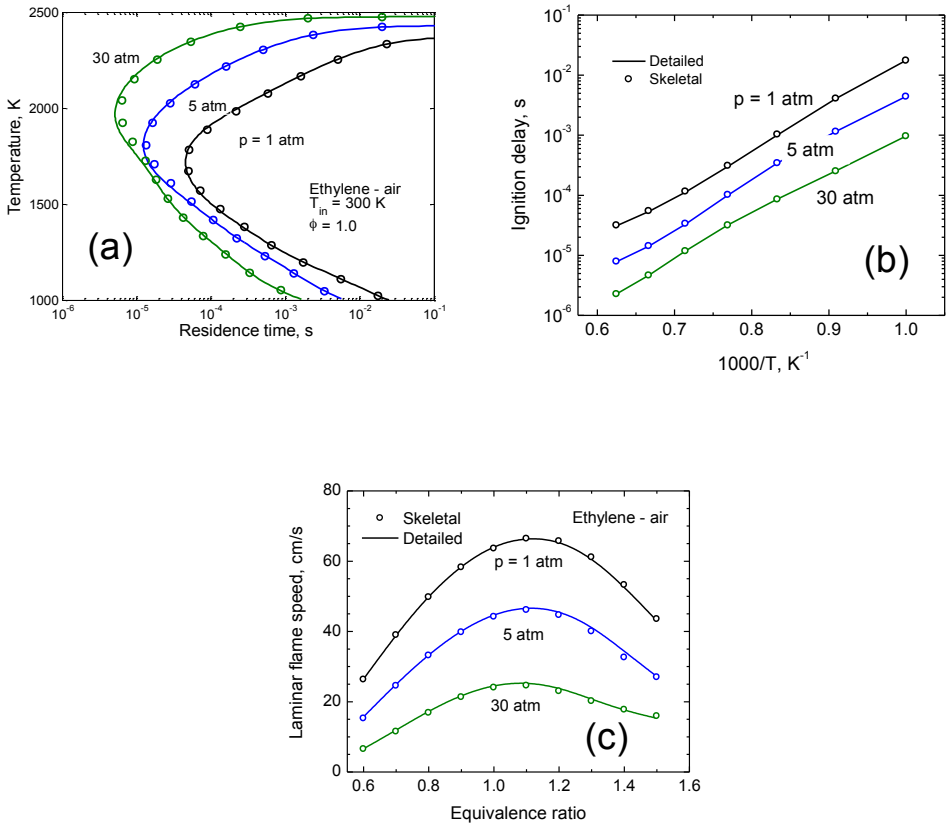

Figure 2-5. Validation of the 34-species skeletal model based on USC-Mech II in (a) PSR, (b) auto-ignition and (c) laminar premixed flame.

Chapter 3 The use of dynamic adaptive chemistry and tabulation in reactive flow simulations

3.1 Introduction

In addition to static model reduction, detailed chemistry can also be simplified on the fly based on the local thermochemical conditions, e.g. by using dynamic adaptive chemistry (DAC). In reactive flow simulations using DAC, the full set of species is transported in the governing equations. At each reaction fractional step, DRG-based methods can be applied to obtain the locally valid skeletal model for each particle/cell. The composition vector, $\boldsymbol{\Phi}$, can then be decomposed as $\boldsymbol{\Phi} \equiv \{\boldsymbol{\Phi}^r, \boldsymbol{\Phi}^u\}$, where $\boldsymbol{\Phi}^r$ includes the mass fractions of the retained species and thermodynamic variables while $\boldsymbol{\Phi}^u$ represents the mass fractions of the unimportant species. The unimportant species are approximated as chemically frozen in the integration step, i.e. $d\boldsymbol{\Phi}^u/dt = 0$. The computational saving is achieved by solving only the ODEs of the size-reduced composition $\boldsymbol{\Phi}^r$ in each reaction fraction step.

To obtain a skeletal model retaining important species and reactions, the reduction method requires search-initiating species, which can be major species in high concentrations, important radicals and/or other species of interest. Starting from these species, depth-first search (DFS) can be employed to identify and retain all the species strongly coupled with the starting species. In previous studies [22-25,39], manually specified starting species are employed in DAC, e.g. the fuel component together with CO, H and NO. In the current study, four starting species are selected based on the local composition. Species H and pollutant NO, by default, are selected if they are present. The remaining species are selected as the most abundant non-inert species in mass. Such automatic procedure is able to dynamically select the important species based on the combustion progress. For example, the fuel species can only be selected as the

starting species in the compression and ignition process in a HCCI application. In a turbulent non-premixed combustion calculation, the starting species significantly vary with the local compositions.

ISAT, as introduced in Section 1.2.2, is another effective approach to speed up chemistry calculations in simulations including direct numerical simulations (DNS), large eddy simulations (LES) or a particle density function (PDF) method. The computational efficiency of ISAT highly depends on the frequency of re-using the tabulated information. For instance, the speedup factor can be as high as 100-1000 for statistically stationary reactive flows [28], while its performance deteriorates when the accessed composition space keeps changing such that the tabulated entries are hardly re-used, e.g. transient auto-ignition in compression ignition engines. In the current study, we explore the possibility to accelerate chemistry calculation using ISAT combined with the DAC strategy.

The combined use of ISAT and DAC was first proposed by Contino et al. [39] for efficient simulations for IC engines with detailed chemistry. In this study, a detailed performance comparison of DAC and ISAT in flame simulations is demonstrated and the coupled ISAT-DAC method is developed. Compared to the previous method, the major improvements in the present method include a more general specification of starting species in DAC and a more accurate approach for sensitivity matrix calculation needed in ISAT.

3.2 Performance of ISAT and DAC

Both ISAT and DAC can speed up the chemistry calculation and be performed on the fly in flame simulations involving a wide range of thermochemical conditions. DAC via DRG with improved selection of starting species is demonstrated in the following. And then ISAT and

DAC are investigated and compared in PDF turbulent flame calculation with various levels of computational complexity. Partially-stirred reactor (PaSR) is used as the test case to study the incurred error in temperature and species concentrations, primarily CO and NO, and the computation efficiency by ISAT and DAC.

3.2.1 Test case: HCCI

In an HCCI engine [40], the homogeneous charge of fuel-air mixture is compressed until auto-ignition occurs. HCCI has great potential benefits of high combustion efficiency and low emissions of NOx and soot due to the low flame temperature in lean combustion. HCCI combustion is used as a test case in the present study to demonstrate the performance of DAC in transient compression ignition of iso-octane/air mixture with equivalence ratio of 0.2. The premixture is initially set at temperature of 850 K, pressure of 13.6 atm and 30 crank-angle-degree (CAD) before the top dead center (TDC). The applied chemistry model is the detailed 874-species LLNL iso-octane model [41]. The engine has peak temperature in the cylinder close to TDC and engine speed of 1000 rpm. In each step of time-integration, the compression/expansion and chemical reaction processes are split into sub-steps using an operator splitting scheme. Each reaction sub-step is set as isobaric, while the pressure will be updated after the reaction step to conserve the mass in the system. The time step of integration is fixed at 10^{-6} s.

Figure 3-1 shows the temperature and species concentration histories calculated with and without DAC. The ignition occurs at approximately 8 CAD before TDC. As the DAC threshold decreases, the results by DAC approach the exact solutions, i.e. the profiles calculated without DAC. The difference in the ignition point, i.e. the crank angle where temperature

reaches 1100 K, is less than 0.2 CAD for $\varepsilon_{\mathrm{DAC}}$ = 0.1 and 1 CAD for $\varepsilon_{\mathrm{DAC}}$ = 0.2, respectively. Meanwhile, the CPU time is significantly reduced by DAC. Speedup factors of 18 and 32 are achieved with $\varepsilon_{\mathrm{DAC}}$ = 0.1 and $\varepsilon_{\mathrm{DAC}}$ = 0.2, respectively.

The adaptive nature of the search-initiating species is illustrated in Fig. 3-2. Here the starting species are H radical and another three non-inert most abundant species in mass fraction. A distinct three-region behavior of HCCI combustion is demonstrated. Before CAD = 712.8 in zone I where the mixture is not ignited, the starting species are iC_8H_{18}, O_2 and other dissociation product of fuel molecule, e.g. iC_4H_8. After that until CAD = 714.8 in zone II, ignition occurs and the fraction of products significantly increases. The starting species are then changed to O_2, CO and H_2O. Finally in zone III where CO has been further oxidized to CO_2 to release a large amount of heat, CO as a starting species is replaced by CO_2. The starting species remain unchanged in the post-combustion phase.

Figure 3-3 further shows the retained species fraction by DRG as a function of CAD in the HCCI simulation. The reduction performance by DRG strongly depends on the combustion states. During the pre-ignition stage (before around 715 CAD), the fraction of the retained species is approximately 10% and 15% for the simulations with $\varepsilon_{\mathrm{DAC}}$ = 0.1 and $\varepsilon_{\mathrm{DAC}}$ = 0.2, respectively. After CAD = 725, where the mixture mostly reaches chemical equilibrium, the fraction is reduced to about 0.02. That is, only around 20 species are retained at the late stage of expansion. Fluctuation in the number of retained species is observed throughout the simulations even though the profiles of temperature and species concentrations are smooth. This is likely induced by the reduction errors of species crossing the threshold value.

It is noted that the computational performance achieved by the current DAC approach is comparable to the performance demonstrated in IC engine simulations [22-24]. With the

adaptive selection of starting species based on the species concentrations, the current approach can also be applied to general reactive flow simulations. Additionally, ISAT results in little reduction in CPU costs in the HCCI test case because the thermos-chemical states keep on evolving and the entries in ISAT table are rarely retrieved. However, the computational load can be reduced by ISAT in multi-dimensional flow simulations where retrieval of spatial states may be possible at the same time.

3.2.2 Test case: PSR

Simulations of PaSR are performed for both premixed and non-premixed combustion of methane/air with the 53-species GRI-Mech 3.0 [42] and 129-species USC-Mech II with updated NOx pathways [36,43], respectively. A PaSR ensembles an individual grid cell in a PDF simulation of a turbulent reacting flow [44]. Various levels of inhomogeneity and computational complexity can be designed in PaSR test cases.

At any time t, a stochastic PaSR simulation involves N_p particles, the ith particle having composition $\mathbf{\Phi}^{(i)}$. The compositions in particles change discontinuously at events of inflow and outflow, which occur at each discrete time instance of $k\Delta t$, where Δt is the specified time step and k is an integer. Between the discrete temporal points, particles compositions evolve due to mixing and chemical reaction, which are treated in separate fractional steps with an operator-splitting scheme. Particles are arranged in pairs and the mixing fractional step for each pair of particles, say p and q, is governed by:

$$\begin{cases} d\Phi^{(p)}/dt = -(\Phi^{(p)} - \Phi^{(q)})/\tau_{mix} \\ d\Phi^{(q)}/dt = -(\Phi^{(q)} - \Phi^{(p)})/\tau_{mix} \end{cases} \tag{3-1}$$

where τ_{mix} is a specified timescale for the pair-wise mixing process, which models the micro-scale molecular diffusion process in turbulent combustion. In the reaction fractional step, each particle evolves independently. With a specified residence time τ_{res}, outflow and inflow select $\frac{1}{2}N_p\Delta t/\tau_{res}$ pairs of particles at random and replace their compositions with inflow's. With a specified pairing timescale τ_{pair}, $\frac{1}{2}N_p\Delta t/\tau_{pair}$ pairs of particles are randomly selected for pairing.

A premixed PaSR involves two inflowing streams: a fresh stream of stoichiometric premixed fuel/air mixture at 600 K, and a pilot stream consisting of the adiabatic equilibrium products of the fresh stream. The mass flow rates of the fresh and pilot streams are in ratios of 0.95:0.05. For the non-premixed PaSR, three streams are involved: a stream of pure fuel at 300 K, a stream of air at 300 K and a pilot stream consisting of the adiabatic equilibrium products of the stoichiometric fuel/air mixture with an initial temperature of 300 K. The ratio of the mass flow rates is 0.05:0.85:0.1. The initial compositions at all the particles at t = 0 are set to be those of the corresponding pilots streams for both premixed and non-premixed cases. The pressure is atmospheric for all the PaSR simulations. Other important parameters involved in the PaSR simulations (listed in Table 3-1) are chosen to produce a good range of compositions to effectively mimic the non-equilibrium combustion with strong turbulence-chemistry interactions. All the PaSRs are simulated for a duration of 10 τ_{res} to reach statistically stationary. The maximum size of the ISAT tables is set to be 500 MB.

Figure 3-4 shows the evolution of the mean temperature and NO mass fractions in the premixed PaSR with 129-spcies USC-Mech II with NOx pathways. A wide range of non-equilibrium conditions are involved as indicated by the large variations in temperature and NO concentrations. The error threshold for ISAT and DAC are $\varepsilon_{\mathrm{ISAT}} = 5\times10^{-6}$ and $\varepsilon_{\mathrm{DAC}} = 0.01$,

respectively. No visible differences are seen for the mean temperature profiles, while minor discrepancies are shown in the mean NO concentration profiles. To further quantify the accuracy, the mean relative percentage errors incurred in temperature and species concentrations over the entire simulations are defined as:

$$\varepsilon_{\psi} = \frac{|\psi^{ID} - \psi^{E}|}{\psi^{ID} + \psi^{E}} \times 100 \tag{3-2}$$

where ψ is a quantity of interest, e.g. temperature or a species concentration, superscript ID indicates the predicted value with ISAT or DAC, and superscript E indicates the exact solution without ISAT or DAC.

Figure 3-5 shows the relative errors of ISAT and DAC in temperature and NO and CO mass fractions as function of speed-up factor in premixed PaSRs. The speed-up factor here is calculated based on the CPU time of the entire simulations rather than that of chemistry integrations. In the simulations with ISAT, more than 98% particle compositions are resolved by retrieving from the ISAT table, such that the speed-up factors for cases using ISAT are much higher than those using DAC at the same level of errors. As shown in Fig. 3-5, when ISAT achieves speed-up factor of 100, only about 0.01%, 0.1% and 10% errors are incurred in temperature, CO and NO mass fractions. In contrast, with the same errors the speed-up factor by DAC is less than 10. The results also reveal that the efficiency achieved by DAC strongly depends on the size of chemistry model, while ISAT is mostly insensitive to the chemistry model. For the cases using 129-species USC-Mech II, DAC achieves speed-up factor of 8 with 0.03%, 0.3% and 10% incurred errors in temperature, CO and NO mass fractions, respectively. However, only speed-up factor of 2 is achieved by DAC at the same level of incurred errors for the cases using 53-species GRI-Mech 3.0. It is because compared to 53-species GRI-Mech 3.0, 129-species USC-Mech II has more room for reduction respect to methane oxidization. Figure

3-6 further confirms the point by showing mean fraction of retained species rr_{spe} and reactions rr_{rxn} by DRG with $\varepsilon_{\mathrm{DAC}}$ = 0.1. It is seen that the reduction by factors of 85% and 90% are achieved in the number of species and reactions, respectively, using 129-species USC-Mech II, however, only factors of 65% and 70% are achieved using 53-species GRI-Mech 3.0.

The evolution of the mean temperature, CO and NO mass fractions for non-premixed PaSR with the 129-species USC-Mech II is further demonstrated in Fig. 3-7. A wide range of compositions are present in the test case as indicated by the larger than 600 K variations in mean temperature history. With the error tolerances set to be $\varepsilon_{\mathrm{ISAT}} = 2\times10^{-5}$ and $\varepsilon_{\mathrm{DAC}}$ = 0.01, the solutions with ISAT and DAC are accurate compared to the exact solution for this challenging case. There are almost no noticeable errors in mean temperature and CO mass fraction profiles, but larger errors for the mean NO mass fractions, showing that the level of incurred error depend on the quantity of interest.

Compared to the premixed cases, non-premixed PaSR is more computationally challenging for ISAT as indicated by the retrieval fraction shown in Table 3-2. For instance, the fraction of retrieval is only 38% for the non-premixed PaSR with $\varepsilon_{\mathrm{ISAT}} = 2\times10^{-5}$, while it is more than 98% for the premixed case with the same threshold value. Consequently, the speed-up factors achieved by ISAT for non-premixed PaSR are less than 3 and are comparable to those by DAC as shown in Fig. 3-8. To achieve the same speedup factor, ISAT incur smaller errors in temperature and CO mass fractions and larger errors in NO mass fractions than those by DAC. For instance, with a speed-up factor of 3, ISAT incurs about 0.1%, 0.9% and 25% errors in temperature, CO and NO mass fraction, respectively, while those by DAC are approximately 0.3%, 9% and 9%, respectively. The differences in the incurred errors are attributed to the different error control strategies adopted in the two methods. DAC controls the

accuracy in reaction rates when performing model reduction whereas ISAT controls normalized two-norm error in compositions. With ISAT, large errors are typically incurred in the species with small concentration such as NO if a uniform scaling factor is employed among all the species.

As demonstrated above, both ISAT and DAC are able to achieve significant saving of computational costs in chemistry calculations with effective error control. The performance of DAC is typically independent of the combustion regimes, e.g. premixed and non-premixed combustion, and its computational efficiency increases with the chemistry model size. Therefore, DAC is suitable for simulations of transient combustion with large chemistry models, e.g. practical engine simulations involving hundreds of species or more. In contrast, ISAT's performance is better for statistically stationary flames, where the calculated solutions can be frequently retrieved from the ISAT tables. Besides, ISAT is most effective for moderate sized chemistry model, e.g. typically those with less than about 50 species, because the ISAT table storage and retrieve time scale with n_s^2. In the next section DAC will be coupled with ISAT for improved performance to accelerate the chemistry calculations.

3.3 ISAT-DAC for highly efficient combustion simulations

A combined method of ISAT and DAC, denoted as ISAT-DAC, for the chemistry calculations in reactive flow simulations is shown in Fig. 3-9. The main differences between the current approach and that in [39] are in the specification of the search-initiating species and in the computation of the sensitivity matrix. The thermochemical composition to be solved, $\boldsymbol{\Phi}$, involves the full set of chemical species in a detailed chemical kinetic model. During the chemistry integration step of Δt with ISAT-DAC, the final composition $\boldsymbol{\Phi}(\Delta t)$ is determined based on the starting composition $\boldsymbol{\Phi}(0)$ at adiabatic and isobaric conditions. An ISAT table

stores the pair of $\boldsymbol{\Phi}(0)$ and $\boldsymbol{\Phi}(\Delta t)$ to be re-used in the future integration. New table entries can be inserted on the fly if needed, through the following procedure:

- Given the initial composition $\boldsymbol{\Phi}(0)$, DRG reduction is performed from the search-initiating species to obtain a skeletal model that is valid for the local thermochemical states. Then the composition is decomposed as $\boldsymbol{\Phi} \equiv \{\boldsymbol{\Phi}^r, \boldsymbol{\Phi}^u\}$ where $\boldsymbol{\Phi}^r$ represents the mass fractions of the retained species together with the thermodynamic variables, and $\boldsymbol{\Phi}^u$ represents the mass fractions of the n_u unimportant species detected by DRG.
- The simplified ODEs for the species retained in the skeletal model are integrated for a time step of Δt to obtain $\boldsymbol{\Phi}(\Delta t)$ with the unimportant species being numerically frozen, i.e. the following set of simplified equations are solved:

$$\begin{cases} d\boldsymbol{\Phi}^r/dt = \boldsymbol{S}^r(\boldsymbol{\Phi}^r, \boldsymbol{\Phi}^u) \\ d\boldsymbol{\Phi}^u/dt = 0 \end{cases} \tag{3-3}$$

where S^r is the chemical source term for the retained species in the local skeletal model. For ISAT tabulation, the gradient matrix $\boldsymbol{A}$ is an important quantity for accurate calculations. In the current ISAT-DAC, the retrieval operations in ISAT are performed based on the full composition. With the retained composition being first in the list, $\boldsymbol{A}$ can be decomposed as:

$$\boldsymbol{A} = \begin{pmatrix} \boldsymbol{A}^{rr} & \boldsymbol{A}^{ru} \\ \boldsymbol{A}^{ur} & \boldsymbol{A}^{uu} \end{pmatrix} \tag{3-4}$$

with $A_{ij}^{rr} \equiv \partial\phi_i^r(\Delta t)/\partial\phi_j^r(0)$, $A_{ij}^{ru} \equiv \partial\phi_i^r(\Delta t)/\partial\phi_j^u(0)$, $A_{ij}^{uu} \equiv \partial\phi_i^u(\Delta t)/\partial\phi_j^u(0)$ and $A_{ij}^{ur} \equiv \partial\phi_i^u(\Delta t)/\partial\phi_j^r(0)$. With DAC, the sensitivity matrix A^{rr} with size of $(n_r+1)\times(n_r+1)$ can be directly obtained from the ODE solvers, e.g. DDASAC [45], while the challenging part is how to construct $\boldsymbol{A}^{ru}, \boldsymbol{A}^{ur}$ and $\boldsymbol{A}^{uu}$. This approach in [39], donated as ISAT-DAC-1, assumes $\boldsymbol{A}^{ru} = \boldsymbol{0}, \boldsymbol{A}^{ur} = \boldsymbol{0}$ and $\boldsymbol{A}^{uu} = \boldsymbol{I}$, where the sensitivities between the retained species and unimportant species are not taken into account. It is found that this method may incur

significant errors when retrieving from the ISAT table due to inaccurate sensitivity matrices. As shown in Fig. 3-10, the solutions by ISAT-DAC-1 with and without DAC have significant differences.

Another approach, denoted as ISAT-DAC-2, is proposed to construct $\boldsymbol{A}$. When the reduced ODEs of Eq. (3-3) are integrated, the full Jacobian matrices $J_{ij}(t) \equiv \partial S_i(\boldsymbol{\Phi}(t))/\partial \phi_j(t)$ are evaluated analytically and recorded at several points in each integration interval as illustrated in Fig. 3-11. These points are chosen to be those where the Jacobian of the reduced systems $J_{ij}^{rr}(t) \equiv \partial S_i^r(\boldsymbol{\Phi}(t))/\partial \phi_j^r(t)$ are required by the ODE solver. The sensitivity matrix can therefore be estimated based on the recorded Jacobian matrices as the product of $\exp(J_k dt_k)$ where dt_k is the k-th time interval and $\boldsymbol{J}_k$ is the Jacobian in that time interval. The computational accuracy is improved since no assumptions are needed for the calculations of the sensitivities. As shown in Fig. 3-10, the temperature profile by ISAT-DAC-2 closely follows with that from the stand-alone ISAT with this improvement.

The ISAT-DAC approach inherits the advantages from both ISAT and DAC for efficient simulations of combustion problems involving complex chemistry. Tabulating reduces the number of expensive ODE integrations by reusing the solutions, while reducing the dimension of equations through local DRG reduction accelerates the required direct integrations. Similar to ISAT, the table in ISAT-DAC is built up on the fly as the simulation being performed. In the current implementation of ISAT-DAC, the storage and retrieval time scale with $(n_s + 1)^2$, since the operations are performed in the full composition space. The averaged computational cost for a query can thus be approximated as:

$$t_Q = t_R(1 - p_F) + t_F^D p_F \tag{3-5}$$

where t_F^D is the reduced CPU time for a direct integration of chemistry if DAC is applied and it also includes the computational overhead in DRG reduction. The speed-up factor in chemistry calculation is:

$$\gamma = \frac{t_F}{t_Q} = \frac{1}{p_F t_F^D / t_F + (1 - p_F) t_R / t_F} \tag{3-6}$$

The ideal speed-up factor with ISAT-DAC is $\gamma = t_F / t_R$, when all the compositions are solved by retrieving from ISAT table. When p_F approaches unity, the ISAT-DAC deteriorates to the stand-alone DAC, i.e. t_F / t_F^D, which can still be significant.

Figure 3-12 shows the incurred errors in temperature and mass fractions of CO and NO as functions of the ISAT error tolerances for the non-premixed PaSR calculated with 129-species USC-Mech II. The reduction threshold is set $\varepsilon_{\mathrm{DAC}}$ = 0.01 in the current ISAT-DAC approach. ISAT error tolerance effectively controls the relative errors with the ISAT-DAC in temperature and species mass fractions for the given reduction threshold value. The errors with ISAT-DAC are attributed to both ISAT and DAC. With the specified reduction threshold of $\varepsilon_{\mathrm{DAC}}$ = 0.01, for a large ε_{ISAT} value, the incurred errors by ISAT are dominant in the coupled approach. The curves from ISAT-DAC are thus close to those from stand-alone ISAT. In contrast, when a small $\varepsilon_{\mathrm{ISAT}}$ value is applied, the errors in temperature and CO concentrations are dominantly attributed to DAC. Nevertheless, the errors in NO with ISAT-DAC are mostly due to ISAT over the whole range of $\varepsilon_{\mathrm{ISAT}}$ at this reduction threshold $\varepsilon_{\mathrm{DAC}}$ = 0.01.

Figure 3-13 compares ISAT-DAC method with stand-alone ISAT. With the same speed-up factor, the ISAT-DAC method achieves higher accuracy in temperature and NO mass fractions than that of stand-alone ISAT. For instance, with the same speed-up factor of 2, about 20% error in NO mass fractions is incurred by the stand-alone ISAT, but only about 9% by ISAT-DAC. To further quantify the computational efficiency, the speed-up factors achieved by

ISAT and ISAT-DAC are summarized in Table 3-3. With the same value of $\varepsilon_{\mathrm{ISAT}}$, ISAT-DAC ($\varepsilon_{\mathrm{DAC}}$ = 0.01) is 30% more efficient than the stand-alone ISAT for the non-premixed PaSR.

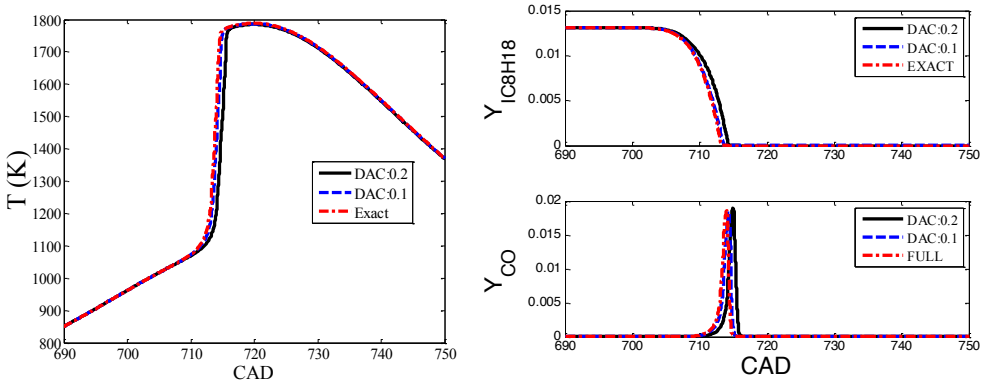

Figure 3-1. Temperature and mass fractions of iso-octane and CO as function of CAD for HCCI combustion of the iso-octane/air mixture with an equivalence ratio of 0.2.

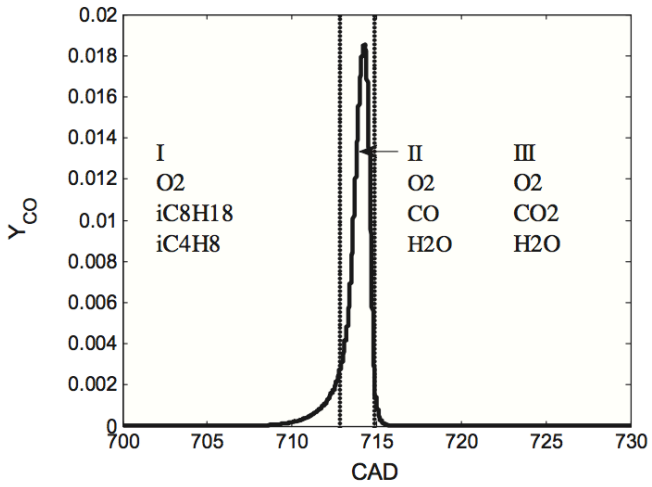

Figure 3-2. The evolution of starting species in the HCCI combustion of an iso-octane/air mixture. The regions with different specification of starting species are marked as I, II and III respectively.

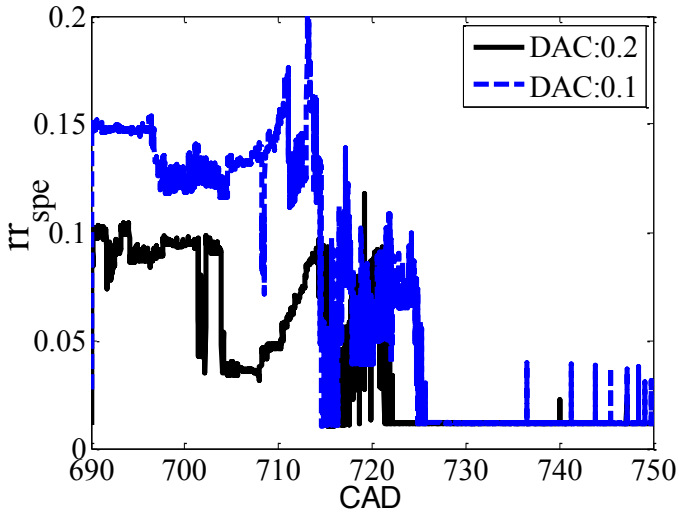

Figure 3-3. The mean fraction of species retained by DRG, rr_{spe}, as a function of CAD for the HCCI combustion of the iso-octane/air mixture with an equivalence ratio of 0.2.

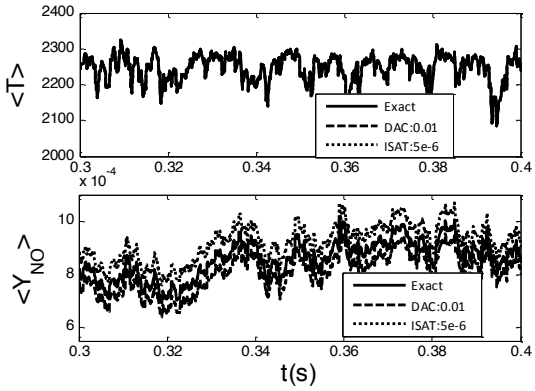

Figure 3-4. The evolution of the mean temperature (K) and mean NO mass fraction in the premixed PaSR case using the 129-species USC-Mech II.

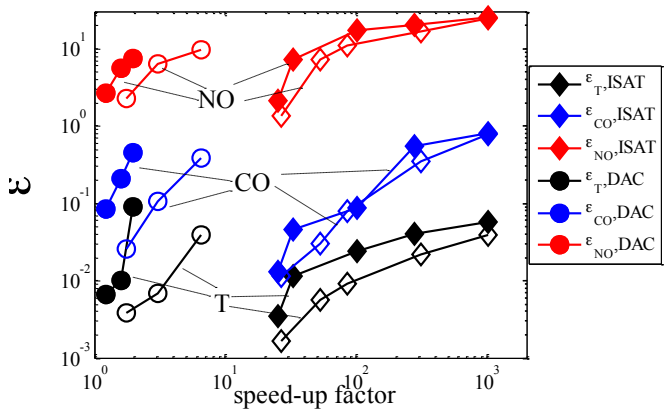

Figure 3-5. The incurred relative percentage errors in temperature (black), CO (blue) and NO (red) as functions of the speedup factor for DAC and ISAT for the premixed PaSR. Closed symbols: with GRI-Mech 3.0; Open symbols: with the 129-species USC-Mech II. The results are obtained with different threshold values of ISAT and DAC.

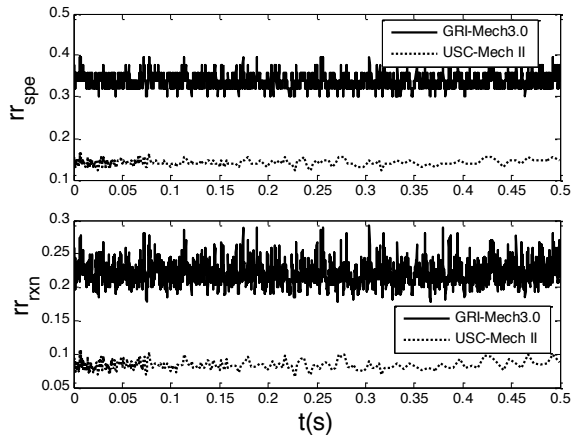

Figure 3-6. The mean fractions of retained species, rr_{spe} and reactions, rr_{rxn} by DRG with $\varepsilon_{\mathrm{DAC}} = 0.1$ for the premixed PaSR.

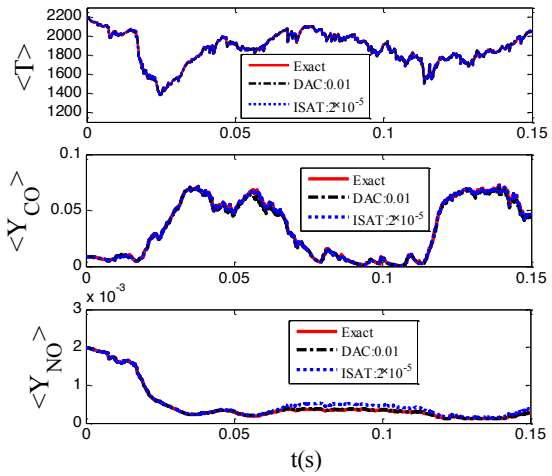

Figure 3-7. The evolution of the mean temperature (K), mean CO mass fraction, and mean NO mass fraction in the non-premixed PaSR using the 129-species USC-Mech II.

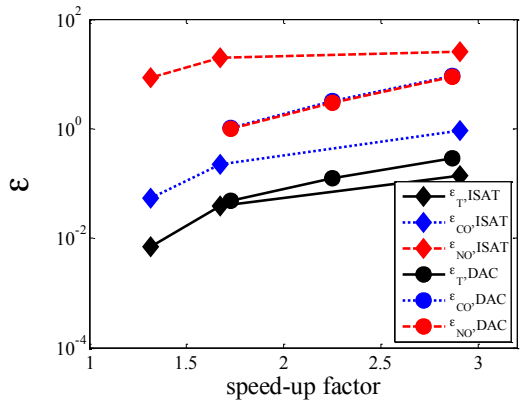

Figure 3-8. Incurred errors in temperature, CO and NO concentrations as functions of the speedup factor for simulations with DAC or ISAT for the non-premixed PaSR using the 129-species USC-Mech II. The results using DAC were obtained with $\varepsilon_{\mathrm{DAC}}$= 0.01, 0.1, 0.2 respectively, and those with ISAT were obtained with $\varepsilon_{\mathrm{ISAT}} = 2\times10^{-5}, 5\times10^{-5}, 1\times10^{-4}$, respectively.

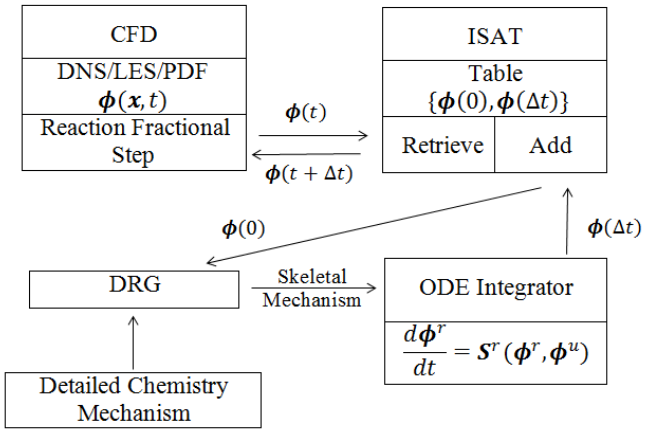

Figure 3-9. Schematic of ISAT-DAC employed in the reaction sub-step.

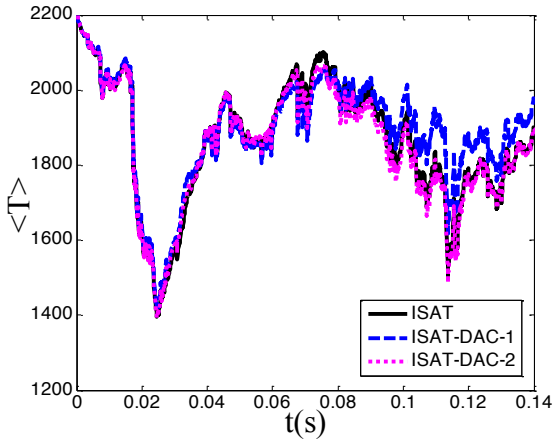

Figure 3-10. The evolution of the mean temperature (K) in the PaSR for the non-premixed case using the 129-species USC-Mech II with $\varepsilon_{\mathrm{ISAT}} = 5\times10^{-4}$ and $\varepsilon_{\mathrm{DAC}} = 0.01$.

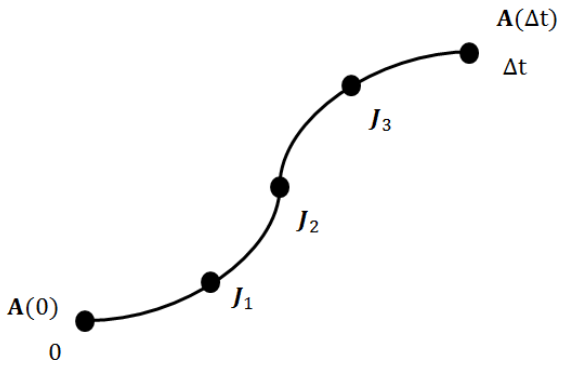

Figure 3-11. The schematic of a reaction mapping from time $t = 0$ to $= \Delta t$ with J_i, i=1, 2, 3, being the Jacobian matrices of the points along the reaction mapping, and A(0) and A(Δt) being the sensitivity matrices at $t = 0$ and $t = \Delta t$, respectively.

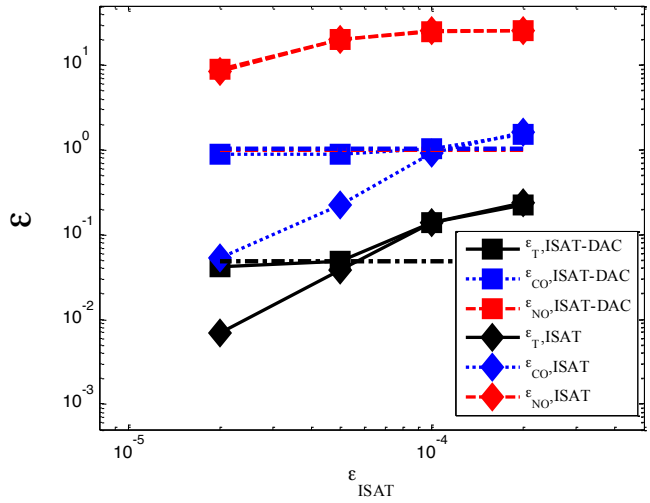

Figure 3-12. The incurred errors in temperature and concentrations of CO and NO as functions of the ISAT error threshold values for the non-premixed PaSR using the 129-species USC-Mech II. The reduction threshold is $\varepsilon_{\mathrm{DAC}} = 0.01$ in ISAT-DAC. The horizontal dash-dot lines represent the incurred errors from the stand-alone DAC method with $\varepsilon_{\mathrm{DAC}} = 0.01$.

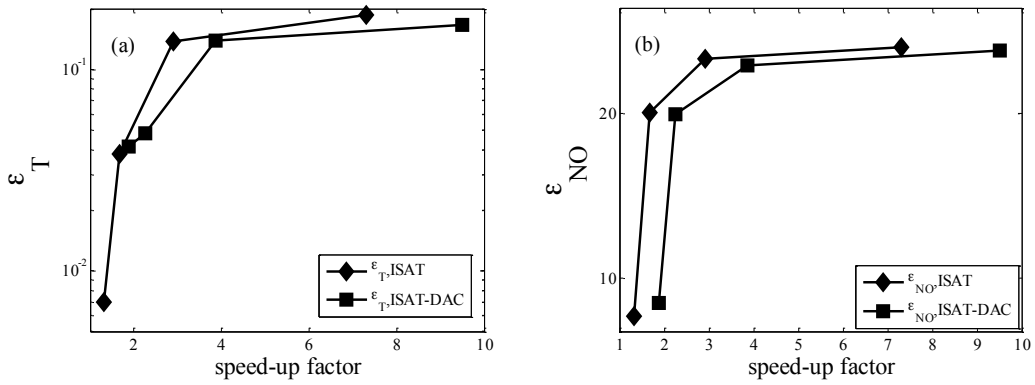

Figure 3-13. The incurred errors in a) temperature and b) NO concentration as functions of the speedup factor for the non-premixed PaSR with USC-Mech II. The data points are obtained with $\varepsilon_{\mathrm{ISAT}}= 2\times10^{-5}$, 5×10^{-5}, 1×10^{-4}, 1.5×10^{-4} , respectively for both ISAT and ISAT-DAC. In ISAT-DAC, the reduction threshold is $\varepsilon_{\mathrm{DAC}} = 0.01$.

Table 3-1. The PaSR parameters used for the test cases for methane/air.

Parameters	τ_{res}	τ_{res}	τ_{pair}	N_p	Δt
Non-premixed	15 ms	1 ms	1 ms	1000	0.1 ms
Premixed	5 ms	1 ms	1 ms	1000	0.1 ms

Table 3-2. The fraction of "retrieve" for the non-premixed PaSR with USC-Mech II.

ε_{ISAT}	1×10^{-4}	5×10^{-5}	2×10^{-5}
p_R	75 %	55 %	38 %

Table 3-3. The speedup factors (SF) achieved by in ISAT and ISAT-DAC for the non-premixed PaSR with USC-Mech II. The reduction threshold in ISAT-DAC is $\varepsilon_{DAC} = 0.01$.

$\varepsilon_{\mathrm{ISAT}}$	2×10^{-5}	5×10^{-5}	1×10^{-4}	1.5×10^{-4}
$\mathrm{SF}_{\mathrm{ISAT}}$	1.32	1.67	2.91	7.31
$\mathrm{SF}_{\mathrm{ISAT-DAC}}$	1.88	2.25	3.86	9.50

Chapter 4 Summaries and future work

A linearized error propagation model (LEP) for skeletal model reduction is developed for steady-state PSR based on Jacobian analysis. The local error control by LEP is compared with DRG and DRGEP. While DRG controls the worst-case error in all the species, DRGEP and LEP control the reduction errors in selected target species. Furthermore, the relative errors in target species, e.g. some important radicals, are smaller in LEP than DRGEP due to the improved approximation of error propagation. Moreover, with the same number of species, the skeletal models obtained by LEP are shown to feature overall the smallest errors among the three tested methods in auto-ignition delay time and species concentrations. A 34-species global skeletal model is developed using LEP over a wide range of parameters for ethylene-air combustion based on the detailed 111-species USC-Mech II. Validations are performed for PSR, auto-ignition and 1-D premixed flame.

The application of ISAT and DAC for efficient simulations with detailed chemical kinetic models is studied for HCCI combustion for iso-octane/air and PaSR for methane/air combustion. It is found that the chemistry calculations are expedited by DAC through local skeletal reduction using DRG, while ISAT speeds up the simulations by reducing the number of direct integrations of ODEs through tabulating and re-using the solutions. Both methods can be performed on the fly and facilitate the use of detailed chemistry with effective error control. For simulations where the tabulated compositions can be frequently retrieved, ISAT is found to be more efficient than DAC. For instance, a speedup factor up to about 1000 is achieved by ISAT in a premixed PaSR with good accuracy in temperature and species concentrations. In contrast, the performance of DAC is mostly independent of combustion nature, e.g. steady or unsteady; premixed or non-premixed and particularly suitable for simulations with large chemistry

models. A speedup factor of approximately 30 is achieved in a simulation for HCCI combustion of lean iso-octane/air mixture with good agreements in temperature and species concentrations.

A combined method of DAC and ISAT, donated as ISAT-DAC, is developed for highly efficient reactive flow simulations with detailed chemistry. ISAT-DAC inherits the advantages of both ISAT and DAC. The number of expensive direct integration of chemistry is largely reduced by tabulation and retrieval of the solutions, and the necessary integrations are also expedited by using the local small skeletal model obtained by DAC. The good error control in temperature and species concentrations by ISAT-DAC is demonstrated. An improvement by ISAT-DAC in the efficiency of ISAT by more than 30% is shown in a computationally challenging non-premixed PaSR of methane/air.

A possible extension of LEP can be the reduction in the computational cost of the LEP method. A potential solution is to apply sparse matrix technique on the error estimation in LEP, i.e. Eq. 2-3. It is also a possible extension to further incorporate other dimension reduction methods, such as rate-controlled constraint equilibrium (RCCE) and the quasi steady state approximations (QSSA), for more efficient chemistry calculations, as RCCE can potentially reduce the table memory and thus enhance the performance of ISAT.

References

[1] C.K. Law, Proc. Combust. Inst. 31 (1) (2007) 1-29
[2] T. Lu, C.K. Law, Proc. Combust. Inst. 30 (1) (2005) 1333-1341
[3] T. Lu, C.K. Law, Combust. Flame 146 (3) (2006) 472-483
[4] T. Lu, C.K. Law, Combust. Flame 144 (1–2) (2006) 24-36
[5] T. Nagy, T. Turányi, Combust. Flame 156 (2) (2009) 417-428
[6] K.E. Niemeyer, C.-J. Sung, M.P. Raju, Combust. Flame 157 (9) (2010) 1760-1770
[7] P. Pepiot-Desjardins, H. Pitsch, Combust. Flame 154 (1–2) (2008) 67-81
[8] W. Sun, Z. Chen, X. Gou, Y. Ju, Combust. Flame 157 (7) (2010) 1298-1307
[9] L. Tosatto, B.A.V. Bennett, M.D. Smooke, Combust. Flame 158 (5) (2011) 820-835
[10] T. Turányi, J. Math. Chem. 5 (3) (1990) 203-248
[11] S. Vajda, T. Turányi, J. Phys. Chem. 90 (8) (1986) 1664-1670
[12] Z. Luo, T. Lu, M.J. Maciaszek, S. Som, D.E. Longman, Energy Fuels 24 (12) (2010) 6283-6293
[13] J.C. Keck, Prog. Energy Combust. Sci. 16 (2) (1990) 125-154
[14] J.C. Keck, D. Gillespie, Combust. Flame 17 (2) (1971) 237-241
[15] S.H. Lam, D.A. Goussis, Int. J. Chem. Kinet. 26 (4) (1994) 461-486
[16] U. Maas, S.B. Pope, Combust. Flame 88 (3–4) (1992) 239-264
[17] Z. Ren, S.B. Pope, Proc. Combust. Inst. 30 (1) (2005) 1293-1300
[18] Z. Ren, S.B. Pope, A. Vladimirsky, J.M. Guckenheimer, J. Chem. Phys. 124 (11) (2006) 114111
[19] T. Lu, C.K. Law, Combust. Flame 154 (4) (2008) 761-774
[20] A.S. Tomlin, M.J. Pilling, T. Turányi, J.H. Merkin, J. Brindley, Combust. Flame 91 (2) (1992) 107-130
[21] T. Turányi, A.S. Tomlin, M.J. Pilling, J. Phys. Chem. 97 (1) (1993) 163-172
[22] L. Liang, J.G. Stevens, J.T. Farrell, Proc. Combust. Inst. 32 (1) (2009) 527-534
[23] L. Liang, J.G. Stevens, S. Raman, J.T. Farrell, Combust. Flame 156 (7) (2009) 1493-1502
[24] Y. Shi, L. Liang, H.-W. Ge, R.D. Reitz, Combust. Theory Model. 14 (1) (2010) 69-89
[25] H. Yang, Z. Ren, T. Lu, G.M. Goldin, Combust. Theory Model. 17 (1) (2013) 167-183
[26] T. Turányi, Comput. Chem. 18 (1) (1994) 45-54
[27] F.C. Christo, A.R. Masri, E.M. Nebot, S.B. Pope, Symposium (International) on Combustion 26 (1) (1996) 43-48
[28] S.B. Pope, Combust. Theory Model. 1 (1) (1997) 41-63
[29] L. Lu, S.B. Pope, J. Comput. Phys. 228 (2) (2009) 361-386
[30] S.R. Tonse, N.W. Moriarty, N.J. Brown, M. Frenklach, Isr. J. Chem. 39 (1) (1999) 97-106
[31] T. Lu, C.K. Law, Prog. Energy Combust. Sci. 35 (2) (2009) 192-215
[32] Z. Luo, "Development of Reduced Chemical Kinetics for Combustion Simulations with Transportation Fuels" (2013). Doctoral Dissertations. Paper 232. (http://digitalcommons.uconn.edu/dissertations/232)
[33] X.L. Zheng, T.F. Lu, C.K. Law, Proc. Combust. Inst. 31 (2007) 367-375
[34] K.E. Niemeyer, C.J. Sung, M.P. Raju, Combust. Flame 157 (9) (2010) 1760-1770
[35] C.K. Law, Combustion physics, Cambridge University Press, 2006.

[36] H. Wang, X. You, A.V. Joshi, D.S. G., A. Laskin, F. Egolfopoulos, C.K. Law USC Mech Version II. High-Temperature Combustion Reaction Model of H2/CO/C1-C4 Compounds. http://ignis.usc.edu/USC_Mech_II.htm, May 2007.
[37] R. Shan, T. Lu, Combust. Flame 159 (6) (2012) 2069-2076
[38] R. Shan, T. Lu, Combust. Flame 161 (7) (2014) 1716-1723
[39] F. Contino, H. Jeanmart, T. Lucchini, G. D'Errico, Proc. Combust. Inst. 33 (2) (2011) 3057-3064
[40] M. Yao, Z. Zheng, H. Liu, Prog. Energy Combust. Sci. 35 (5) (2009) 398-437
[41] H.J. Curran, P. Gaffuri, W.J. Pitz, C.K. Westbrook, Combust. Flame 129 (3) (2002) 253-280
[42] G.P. Smith, D.M. Golden, M. Frenklach, N.W. Moriarty, B. Eiteneer, M. Goldenberg, C.T. Bowman, R.K. Hanson, S. Song, W.C. Gardiner, V.V. Lissianski, Z. Qin, (<http://www.me.berkeley.edu/gri_mech/>. <http://www.me.berkeley.edu/gri_mech/>.)
[43] Z. Luo, T. Lu, J. Liu, Combust. Flame 158 (7) (2011) 1245-1254
[44] D.C. Haworth, Prog. Energy Combust. Sci. 36 (2) (2010) 168-259
[45] M. Caracotsios, W.E. Stewart, Comput. Chem. Eng. 9 (4) (1985) 359-365